12th International Symposium on Turbulence and Shear Flow Phenomena (TSFP12)
Osaka, Japan (Online), July 19-22, 2022

TURBULENT TRANSONIC BUFFET ONSET PREDICTION ON THE NASA COMMON RESEARCH MODEL VIA GLOBAL STABILITY ANALYSIS

Andrea Sansica
Aircraft Lifecycle Innovation Hub, Digital Integrated Design Technology Team
Aviation Technology Directorate
Japan Aerospace Exploration Agency
Chofu Aerospace Center, Chofu, Tokyo, 182-8522 Japan
sansica.andrea@jaxa.jp

Atsushi Hashimoto
Aircraft Lifecycle Innovation Hub, Digital Integrated Design Technology Team
Aviation Technology Directorate
Japan Aerospace Exploration Agency
Chofu Aerospace Center, Chofu, Tokyo, 182-8522 Japan
hashimoto.atsushi@jaxa.jp

ABSTRACT

A fully-3D global stability analysis (GSA) is performed on the NASA Common Research Model (CRM) body-wing-tail geometry. Differently from other methods present in the literature, the combination of the solver linearization approach and modal decomposition based on time-stepper and Arnoldi methods allows to relax the RAM requirements and perform an angle of attack (AoA) parametric study to determine buffet onset. The RANS solutions, buffet onset and frequencies predicted by GSA are all in good agreement with the experiments carried out at JAXA's 2m×2m Transonic Wind Tunnel. While only a 3D buffet cells mode is found unstable in the vicinity of the onset, additional modes appear at higher AoAs. Besides a 2D low-frequency mode, another high-frequency unstable mode is localized in the separated region at the wing-body junction. This is the first fully-3D GSA study able to predict and characterize buffet onset over a large range of AoAs.

INTRODUCTION

For commercial aviation, the interaction between shock-waves and boundary-layers represents a critical aspect for both design and certification phases. A specific type of shock-wave and turbulent boundary-layer interaction is the so-called turbulent transonic buffet. Turbulent transonic buffet is a three-dimensional (3D) phenomenon consisting of two distinct instabilities (Lee, 2001; Giannelis *et al.*, 2017). The first one is related to the two-dimensional (2D) streamwise shock oscillations, that cause the shock-wave forming on the wing suction side to move periodically back and forth in the streamwise direction. The second one concerns the 3D cross-flow propagation of the so-called buffet cells. These instabilities can origin wing vibrations and represent a limiting factor for the flight envelope. Due to the coexistence of 3D effects, separated turbulent boundary-layers and unsteady shock-waves, buffet represents a very challenging problem and, despite the past and recent experimental and numerical studies, the governing mechanisms remain unclear. Numerical simulations particularly suffer of the complexity associated to the buffet phenomenon and computationally inexpensive tools are constantly sought for its characterization and prediction.

Global stability analysis (GSA) has recently proved a good alternative to classical unsteady RANS (URANS) simulations for buffet prediction (Crouch *et al.*, 2009, 2019; Paladini *et al.*, 2019; Sansica *et al.*, 2022). However, due to the high RAM memory costs associated with the resolution of the linearized dynamical system eigenvalue problem, the configurations studied were simplified to 2D aerofoils or periodic extruded wings. Timme (2020) recently performed a fully-3D GSA study on the NASA Common Research Model (CRM), but only two angles of attack (AoAs) were investigated on an 8 million cells grid. While a 3D buffet-cells mode was found to be unstable, no evidence of a 2D shock-oscillation mode was given.

In the present work, a fully-3D GSA study is carried out with the intent to predict buffet onset for the NASA CRM body-wing-tail configuration. Due to the combination of a time-stepper and an Arnoldi method, the RAM requirements are relaxed and a parametric studied on the AoA is performed to predict the buffet onset on grid resolutions spanning from 3 to 30 million cells. Buffet is characterized both in the vicinity and far from the onset and the numerical results are compared with the experiments carried out at the Japan Aerospace Exploration Agency (JAXA).

1 PROBLEM FORMULATION

The compressible 3D RANS equations for a perfect gas can be written using Boussinesq hypothesis in the non-dimensional form as:

$$\frac{\partial \mathbf{q}}{\partial t} = \mathcal{N}(\mathbf{q}), \tag{1}$$

where $\mathbf{q} = [\rho, \rho\mathbf{u}, \rho E, \rho\nu_t]^T$ is the state vector in the conservative form (with ρ, $\mathbf{u}$, E and ν_t being fluid density, velocity vector, total energy, and kinematic turbulent viscosity, respectively) and t is the time. The differential nonlinear RANS operator $\mathscr{N}$ can be explicitly expanded as

$$\mathscr{N}(\mathbf{q}) = -\begin{pmatrix} \rho\mathbf{u} \\ \rho\mathbf{u}\otimes\mathbf{u} + p\mathbf{I} - \boldsymbol{\tau} - \boldsymbol{\tau}_R \\ \rho E\mathbf{u} + p\mathbf{u} - \boldsymbol{\tau}\mathbf{u} - \boldsymbol{\tau}_R\mathbf{u} + \mathbf{q} + \mathbf{q}_R \\ \rho\nu_t\mathbf{u} - \frac{\mu+\rho\nu_t}{\sigma_M}\nabla\nu_t + \mathscr{S}_M \end{pmatrix} \tag{2}$$

with

$$\begin{gathered} p = (\gamma-1)\rho E - \tfrac{1}{2}\mathbf{u}\cdot\mathbf{u} \\ \boldsymbol{\tau} = \mu\left[(\nabla\otimes\mathbf{u} + \nabla\otimes\mathbf{u}^T) - \tfrac{2}{3}(\nabla\cdot\mathbf{u})\mathbf{I}\right] \\ \boldsymbol{\tau}_R = \mu_t\left[(\nabla\otimes\mathbf{u} + \nabla\otimes\mathbf{u}^T) - \tfrac{2}{3}(\nabla\cdot\mathbf{u})\mathbf{I}\right] \\ \mathbf{q} = -\frac{\mu C_p}{Pr}\nabla T \\ \mathbf{q}_R = -\frac{\mu_t C_p}{Pr_t}\nabla T \end{gathered} \tag{3}$$

being p the pressure, $\boldsymbol{\tau}$ the stress tensor, $\boldsymbol{\tau}_R$ the Reynolds stress tensor, C_p the heat capacity at constant pressure, μ the dynamic viscosity, μ_t the eddy viscosity, Pr and Pr_t the classical and turbulent Prantdl numbers, T the temperature, $\mathbf{q}$ the heat flux and $\mathbf{q}_R$ the flux of diffusion of turbulent enthaply. The Prandtl numbers are considered constant and equal to $Pr = 0.72$ and $Pr_t = 0.90$. The dynamic viscosity is assumed to follow Sutherland's law as

$$\mu = T^{3/2}\frac{1+T_s}{T+T_s} \tag{4}$$

where $T_s = 110.4K/T^*_{i,\infty}$, with $T^*_{i,\infty}$ the dimensional free-stream stagnation temperature (the superscript * indicates dimensional quantities). The array of the streamwise, vertical and transverse directions is indicated by $\mathbf{x} = [x, y, z]^T$. Note that all variables are Reynolds averaged, except for $\mathbf{u}$ and E that are Favre (density-weighted) averaged. The formulations of the coefficient σ_M and the turbulent source terms $\mathscr{S}_M$ depend on the turbulence model.

1.1 Stability Problem

The GSA problem is based upon the use of the linearized RANS equations. The first step to obtain this linearized set of equations is to assume that the nonlinear system in Eq. (1) admits an equilibrium solution, $\mathbf{q}_b$, defined by $\mathscr{N}(\mathbf{q}_b) = 0$ and referred to as fixed point or base flow. In this case, the steady RANS solution corresponds to the base flow. The standard small perturbation technique is used to decompose the instantaneous flow into base flow and small disturbances $\mathbf{q}(\mathbf{x},t) = \mathbf{q}_b(\mathbf{x}) + \varepsilon\mathbf{q}'(\mathbf{x},t)$, with $\varepsilon \ll 1$. By assuming that the perturbations are infinitesimal, all nonlinear fluctuating terms are ignored and the linearized RANS equations can be written as

$$\frac{\partial\mathbf{q}'}{\partial t} = \mathscr{L}\mathbf{q}', \tag{5}$$

where $\mathbf{q}' = \left[\rho', \rho'\mathbf{u}_b + \rho_b\mathbf{u}', \rho' E_b + \rho_b E', \rho'\nu_{t,b} + \rho_b\nu_t'\right]^T$ is the state vector of conservative perturbation variables and $\mathscr{L} = \partial\mathscr{N}/\partial\mathbf{q}\,|_{\mathbf{q}_b}$ is the Jacobian operator obtained by linearizing the RANS operator $\mathscr{N}$ around the base flow $\mathbf{q}_b$. By choosing the normal mode or wave solution $\mathbf{q}'(\mathbf{x},t) = \widehat{\mathbf{q}}(\mathbf{x})\exp(\lambda t) + c.c.$, the eigenproblem $\mathscr{L}\widehat{\mathbf{q}} = \lambda\widehat{\mathbf{q}}$ is obtained. The complex eigenvalue can be split in its real and imaginary parts $\lambda = \sigma + i\omega$, where σ is the temporal growth rate and ω the angular frequency. While the angular frequency characterizes the oscillatory behavior, the temporal growth rate indicates whether the equilibrium state bifurcates to another solution. This bifurcation is expressed in a linear framework by the existence of eigenmodes with a corresponding positive growth rate.

2 NUMERICAL METHOD

While the calculation of the base flow solutions is carried out by using a classical RANS (nonlinear) solver, the global stability analysis requires a URANS linearized solver. The characteristics and numerical strategies used for both solvers are described below.

2.1 Nonlinear Solver

As RANS nonlinear solver, JAXA's unstructured-grid flow solver FaSTAR (Hashimoto *et al.*, 2012; Ishida *et al.*, 2017) is used. The governing equations are the compressible Navier-Stokes equations. The cell-center finite volume method is used for the discretization. The numerical flux is computed with the SLAU scheme and a dual-time stepping method (Visbal & Gordnier, 2000) is used to perform an accurate time calculation with an implicit time integration. The LU-SGS scheme (Sharov & Nakahashi, 1998) is used for the pseudo time sub-iterations and the physical time derivative is approximated by a three-point backward difference method. The Spalart-Allmaras turbulence model (Spalart & Allmaras, 1992) with rotation correction (SA-R) (Dacles-Mariani *et al.*, 1995) and quadratic constitutive relation 2000 version (Spalart, 2000) is used to close the averaged Reynolds stresses. The boundary conditions used are: no-slip velocity and adiabatic temperature on the aicraft walls; far-field boundary conditions are employed at the lateral boundaries and the AoA is applied at the inflow of the numerical domain. All steady solutions are computed by using a large Courant-Friedrichs-Lewy (CFL) number equal to 10. The selective frequency damping (SFD) method (Richez *et al.*, 2016; Akervik *et al.*, 2006) is used to further converge the steady fixed point solution and filter any possible unsteadiness.

2.2 Linearized Solver

The expression of $\mathscr{L}\mathbf{q}'$ is extremely complicated and would mean a lengthy implementation and modification of the existing nonlinear version of FaSTAR. To avoid this, a strategy based on a finite difference method consists of using the nonlinear solver in a black box manner and approximate $\mathscr{L}\mathbf{q}'$ via repeated evaluation of the residual function $\mathscr{N}(\mathbf{q})$. A Taylor series expansion with a first order approximation allows then

$$\mathscr{L}\mathbf{q}' = \frac{1}{\varepsilon}[\mathscr{N}(\mathbf{q}_b + \varepsilon\mathbf{q}') - \mathscr{N}(\mathbf{q}_b)], \tag{6}$$

with ε being a small constant. This method and selection of the ε constant are further discussed in (Tezuka & Suzuki, 2006; Mettot *et al.*, 2014). A matrix-free method (Edwards *et al.*, 1994; Bagheri *et al.*, 2009) is then used to solve the eigenproblem $\mathscr{L}\widehat{\mathbf{q}} = \lambda\widehat{\mathbf{q}}$. Being $\mathbf{L}$ the discrete form of $\mathscr{L}$, it is possible to introduce the exponential propagator $\mathbf{M} = \exp(\mathbf{L}\Delta T)$

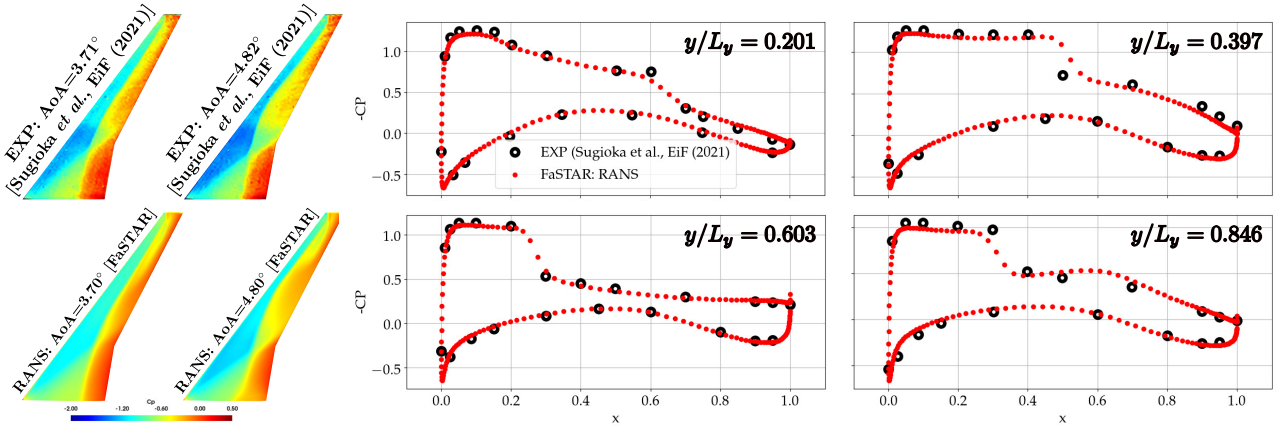

Figure 1. Experimental PSP and RANS pressure coefficient contours on the main wing (left) and pressure distributions at different spanwise wing sections for AoA = 4.8° (right).

that linearly advances the perturbation solution in time as $\mathbf{q}'(t^{n+1}) = \mathbf{M}\mathbf{q}'(t^n)$, with $t^{n+1} = t^n + \Delta T$. An Arnoldi algorithm (Arnoldi, 1951; Lehoucq *et al.*, 1997; Barkley *et al.*, 2008) is coupled to the linearized solver (Loiseau *et al.*, 2014; Guiho *et al.*, 2016; Sansica *et al.*, 2018) to extract the leading eigenmodes of **M**. While all conservative quantities are perturbed, the perturbation eddy viscosity is not included in the linearized snapshot matrix (Krylov base).

The linearized solver, referred to as FaSTAR-GSA, has been validated against the literature for 2D laminar incompressible cylinders, 2D turbulent transonic buffet and applied to fully-3D unswept and swept wings in the presence of lateral walls (Sansica *et al.*, 2022). The combination of the solver linearization approach with the modal decomposition technique selected allows to: a) leverage all FaSTAR's high-performance computing features for complex geometries, b) be flexible in the selection of spatial schemes and turbulence models (opening up to sensitivity studies) and c) investigate high-resolution numerical grids.

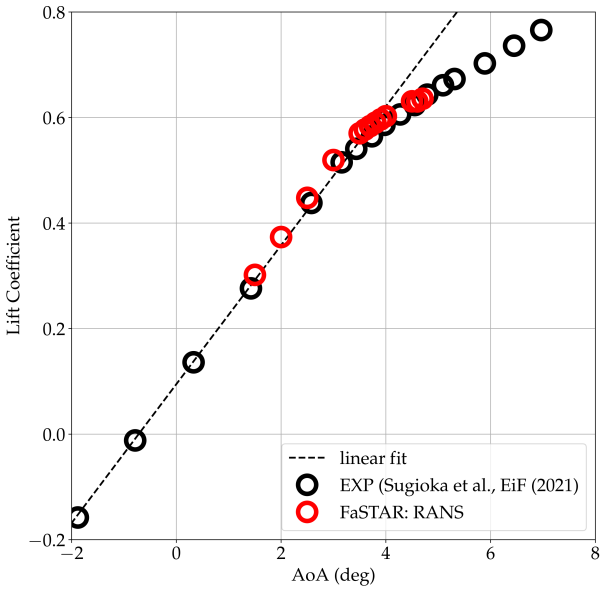

Figure 2. Lift-coefficient based buffet onset prediction.

FLOW CONDITIONS AND NUMERICAL GRID

The numerical flow conditions are selected to match the experiments carried out at JAXA's 2m×2m Transonic Wind Tunnel (JTWT1) on the NASA CRM at a Mach number of 0.85 and a chord Reynolds number of 2.27×10^6 by Sugioka *et al.* (2021). Buffet onset was experimentally determined by using the lift-coefficient method and wing-strain gauge measurements at AoA ≈ 3.5 and 3.7°, respectively. Unsteady pressure-sensitive paint (PSP) and pressure taps at different wing sections were used to characterize the pressure fluctuations. Buffet cells were observed in a frequency range of $400-850\,Hz$ (or, in nondimensional Strouhal number, St≈0.2-0.5).

The geometry selected is the NASA CRM model in the body-wing-tail configuration. The main wing considers the deformation measured experimentally at AoA = 2.94°. Coarse (≈ 2.8×10^6 cells), medium (≈ 9×10^6 cells) and fine (≈ 30×10^6 cells) resolution grids were considered. For brevity, the results presented here only correspond to the medium resolution grid. Geometries and numerical grids are openly accessible on JAXA's Aerodynamics Prediction Challenge (APC) website at https://cfdws.chofu.jaxa.jp/apc/grids/nasa-crm/APC1-3/wbh/upacs/fastar/.

RESULTS

For the medium resolution grid, a total of 16 AoAs are spanned between 1.5 and 4.8°. The RANS solutions (later used as base flows for the GSA) are first compared with the experimental time-averaged PSP and pressure taps measurements. The buffet onset is then calculated by using two criteria, namely the lift-coefficient method and the GSA study.

Base flow solutions

The pressure coefficient, C_P, contours on the main wing at AoA = 3.7 and 4.8° obtained with FaSTAR (left-bottom) are compared with the experimental time-averaged PSP by Sugioka *et al.* (2021) (left-top) in figure 1. The C_P distributions at different spanwise sections of the main wing (available at https://cfdws.chofu.jaxa.jp/apc/apc3) are also compared with the experiments performed for JAXA's APC-3 on the same flow conditions and geometry of Sugioka *et al.* (2021) for the AoA = 4.8°. The solutions are in reasonable good agreement with the experiments and are used as base flows for the GSA.

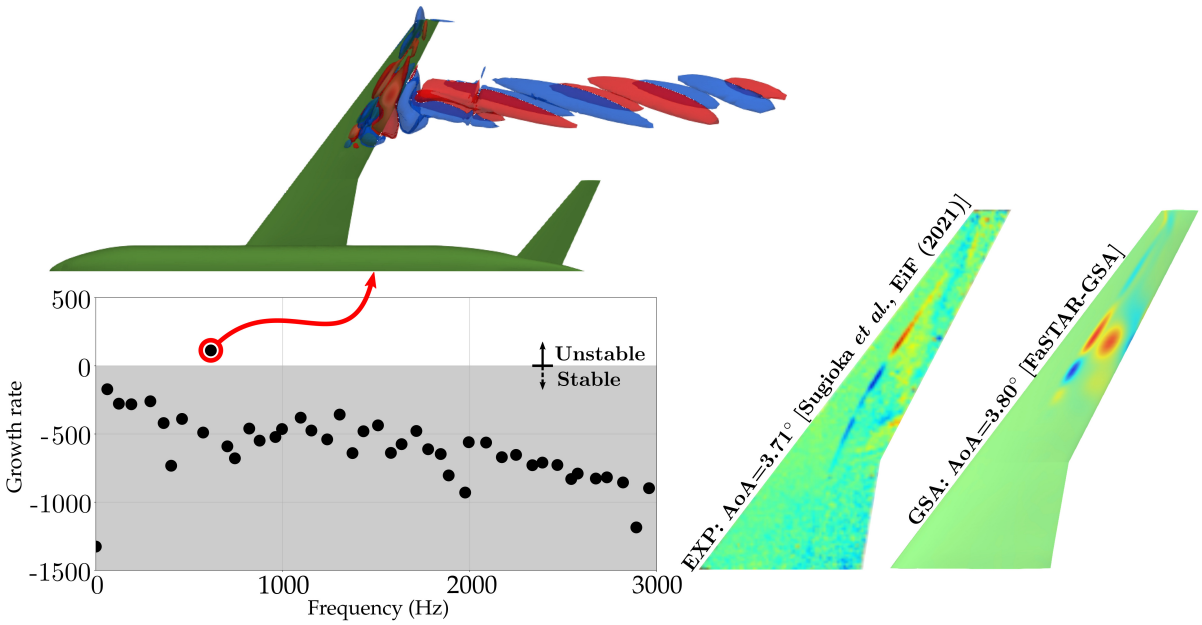

Figure 3. GSA spectrum and unstable mode at AoA = 3.8°. A comparison with the experimental C_P fluctuations is given on the right.

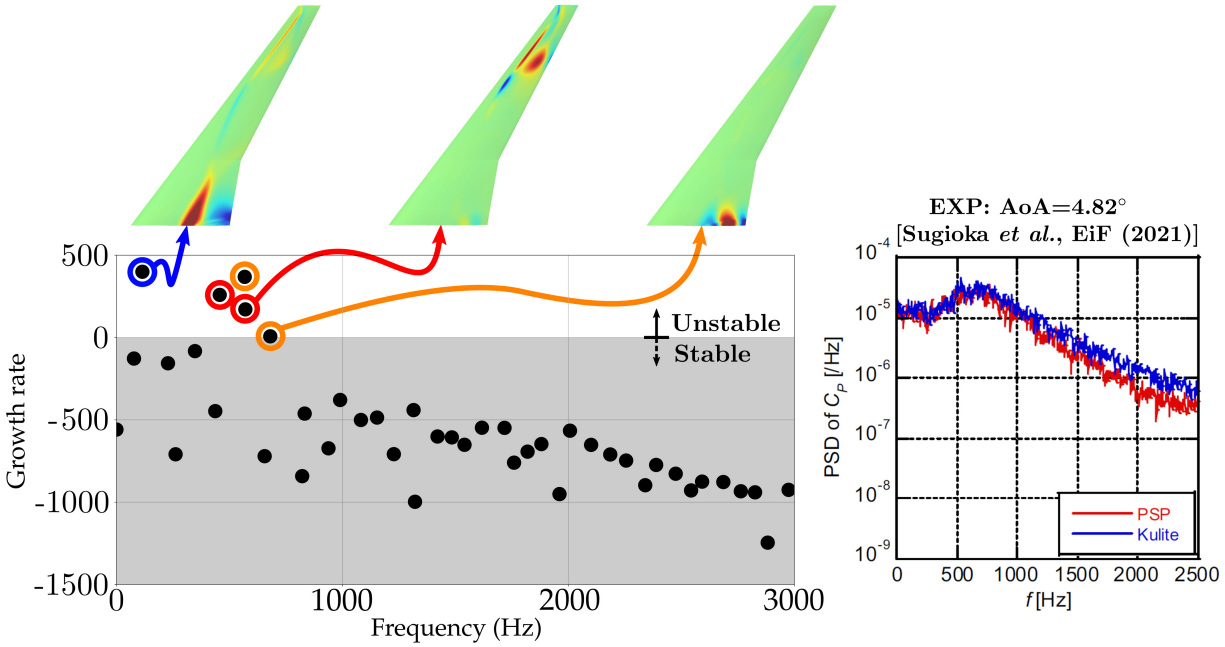

Figure 4. GSA spectrum and unstable modes at AoA = 4.8°. The experimental PSD of C_P is given on the right.

Lift-coefficient based buffet onset prediction

The lift-coefficient method is a criteria commonly used in the industry and consists of determining the buffet onset by detecting a change of the lift-coefficient curve gradient as a function of the AoA. As shown in figure 2, a linear fit (dashed line) can be used to approximate the lift-coefficient at low angles. A shift of $\Delta = 0.1°$ to the right hand side of the linear fit is then used to determine buffet onset. Both experiments (black empty circles) and RANS solution (red empty circles) predict buffet onset around AoA = 3.5°.

GSA based buffet onset prediction

A second criteria commonly used in the industry is based on the calculation of a buffet intensity coefficient based on experimental strain gauge measurements. By using this method, Sugioka *et al.* (2021) found a buffet onset at AoA = 3.7°. The strain gauge buffet onset is selected to be compared with the GSA based predictions. Similarly to what concluded in the experiments, GSA predicts buffet onset around AoA= 3.75°. Near the onset at AoA= 3.8°, GSA predicts only one unstable mode at $f = 615\,Hz$ ($St \approx 0.3$), as shown in figure 3. In close agreement with the experimental C_P fluctuations, this unstable mode corresponds to the outboard convection of 3D buffet cells. The mode shape is also in very good agreement with the GSA results by Timme (2020). Farther from the onset at AoA= 4.8°, GSA predicts several unstable modes in the same frequency bump range found in the experiments (figure 4). As well as the buffet cells mode, a second type of high-frequency mode is localized in the wing-junction separation region. A 2D low-frequency mode at $f = 115\,Hz$ ($St \approx 0.06$) is

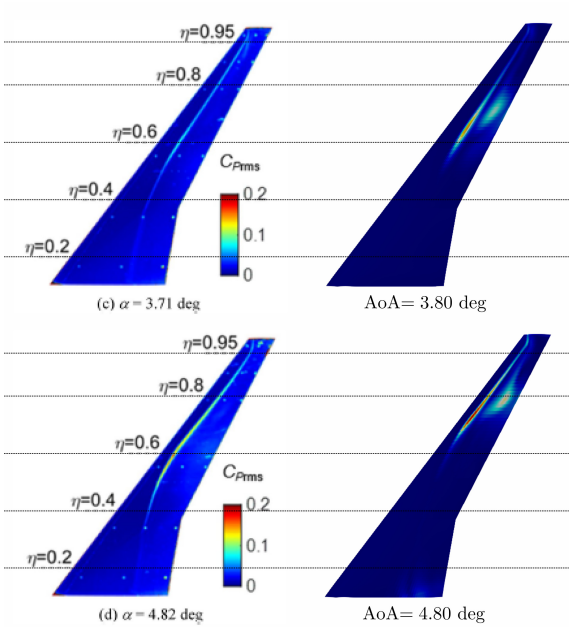

Figure 5. Comparison between the experimental $C_{P,rms}$ and the GSA unstable mode eigen-pressure amplitude at AoA = 3.7° (top) and 4.8° (bottom).

also found. By looking at the experimental root-mean-square pressure coefficient fluctuations $C_{P,rms}$ in comparison with the eigen-pressure amplitude distribution associated with the GSA unstable buffet cells mode (figure 5), it should be however noted that further away from the buffet onset the agreement between experiments and GSA deteriorates. Near the onset, the shock oscillation amplitude is small and the RANS solution used for the GSA study well approximates the time-averaged flow field. However, for higher angles the shock oscillation amplitude increases and the difference between the steady RANS solution and the time-averaged flow field result in larger discrepancies.

Sensitivity tests

The sensitivity of RANS solutions and GSA results to grid resolution and turbulence model is investigated. For the grid sensitivity, coarse ($\approx 2.8\times10^6$ cells), medium ($\approx 9\times10^6$ cells) and fine ($\approx 30\times10^6$ cells) grids are investigated. For the turbulence model sensitivity, the SA-R-QCR200 is compared against the 2-equation Menter Shear Stress Transport (SST) model (Menter, 1994). Additionally for the GSA study, the sensitivity to the perturbation amplitude ε (see section 2.2) is also analyzed by selecting $\varepsilon = 1\times10^{-1}$, $\varepsilon = 5\times10^{-2}$ and $\varepsilon = 1\times10^{-2}$. The RANS solutions (and therefore the lift-coefficient based buffet onset prediction criteria) are nearly insensitive to grid resolution and turbulence model tests. For the GSA study, while turbulence model and perturbation amplitude show no significant sensitivity, the buffet onset is predicted at AoA = 3.75° for both coarse and medium resolution grids and at AoA = 4.15° for the fine resolution grid. Table 1 shows a summary of the experimental and numerical onset predictions using the different methods described above. The sensitivity tests are accounted for by reporting the onset AoA lower and upper limits.

Table 1. Buffet onset AoA calculated with different criteria for both experiments (EXP) and numerical simulations (CFD). Lower and upper limits are reported to account for the sensitivity tests. The experimental results are taken from Sugioka *et al.* (2021).

	EXP	CFD
Lift	3.50°	3.50 – 4.00°
Strain	3.70°	×
GSA	×	3.75 – 4.15°
ONSET	3.50 – 3.70°	3.50 – 4.15°

CONCLUSIONS

The work here presented is the first fully-3D GSA investigation aimed at characterizing buffet over a large range of AoAs and predicting its onset. By calculating the lift-coefficient with JAXA's RANS solver, the widely used in the industry lift-coefficient criteria is used to predict buffet onset. The GSA based buffet prediction is then compared with the experimental strain gauge measurements carried out at JAXA JTWT1 wind tunnel (Sugioka *et al.*, 2021). An overall good agreement exists with the experimental findings, although the numerical agreement with the PSP-based perturbation distributions deteriorates farther away from the onset.

The agreement with the experiments shows the possibility to use GSA as a computationally cheaper alternative to more classical approaches (i. e. URANS) for buffet onset prediction. To obtain converged information on buffet onset, the estimated computational time saving with GSA with respect to URANS is in fact of about one order of magnitude. By including sensitivities to grid and turbulence modeling, the GSA-based buffet onset prediction can be a valuable tool during both design and certification phases of commercial aircrafts.

ACKNOWLEDGMENTS

The numerical work was partially supported by JSPS KAKENHI Grant-in-Aid for Early-Career Scientists 20K14953.

REFERENCES

Akervik, E., Brandt, L., Henningson, D. S., Hoepffner, J., Marxen, O. & Schlatter, P. 2006 Steady solutions of the Navier-Stokes equations by selective frequency damping. *Physics of Fluids* **18**, 068102.

Arnoldi, W. E. 1951 The principle of minimized iterations in the solution of the matrix eigenvalue problem. *Quarterly of Applied Mathematics* **9**.

Bagheri, S., Åkervik, E., Brandt, L. & Henningson, D. S. 2009 Matrix-free methods for the stability and control of boundary layers. *AIAA Journal* **45**.

Barkley, D., Blackburn, H. M. & Sherwin, S. J. 2008 Direct optimal growth analysis for timesteppers. *International for numerical methods in fluids* **57**, 1435–1458.

Crouch, J. D., Garbaruk, A., Magidov, D. & Travin, A. 2009 Origin of transonic buffet on aerofoils. *Journal of Fluid Mechanics* **628**, 357–369.

Crouch, J. D., Garbaruk, A. & Strelets, M. 2019 Global instability in the onset of transonic-wing buffet. *Journal of Fluid Mechanics* **881**, 3–22.

Dacles-Mariani, J, Zilliac, G. G., Chow, J. S. & Bradshaw, P. 1995 Numerical/experimental study of a wingtip vortex in the near field. *AIAA Journal* **33**, 1561–1568.

Edwards, W. S., Tuckerman, L. S., Friesner, R. A. & Sorensen, D. 1994 Krylov methods for the incompressible Navier-Stokes equations. *Journal of Computational Physics* **110**, 82–101.

Giannelis, N. F., Vio, G. A. & Levinski, O. 2017 A review of recent developments in the understanding of transonic shock buffet. *Progress in Aerospace Sciences* **92**, 39–84.

Guiho, F., Alizard, F. & Robinet, J.-C. 2016 Instabilities in oblique shock wave/laminar boundary-layer interactions. *Journal of Fluid Mechanics* **789**, 1–35.

Hashimoto, A., Murakami, K., Aoyama, T., Ishiko, K., Hishida, M., Sakashita, M. & Lahur, P. 2012 Toward the fastest unstructured CFD code 'FaSTAR'. *AIAA Paper 2012-1075* .

Ishida, T., Hashimoto, A., Ohmichi, Y., Aoyama, T. & Takekawa, K. 2017 Transonic buffet simulation over NASA-CRM by unsteady-FaSTAR code. *AIAA Paper 2017-0494* .

Lee, B. H. K. 2001 Self-sustained shock oscillations on airfoils at transonic speeds. *Progress in Aerospace Sciences* **37**, 147–196.

Lehoucq, R. B., Sorensen, D. C. & Yang, C. 1997 ARPACK user's guide: solution of large scale eigenvalue problems with implicitly restarted Arnoldi methods. *Technical Note* .

Loiseau, J.-C., Robinet, J.-C., Cherubini, S. & Leriche, E. 2014 Investigation of the roughness-induced transition: global stability analyses and direct numerical simulations. *Journal of Fluid Mechanics* **760**, 175–211.

Menter, F. R. 1994 Two-equation eddy-viscosity turbulence models for engineering applications. *AIAA Journal* **32**, 1598–1605.

Mettot, C., Renac, F. & Sipp, D. 2014 Computation of eigenvalue sensitivity to base flow modifications in a discrete framework: Application to open-loop control. *Journal of Computational Physics* **269**, 234–258.

Paladini, E., Beneddine, S., Dandois, J., Sipp, D. & Robinet, J.-Ch. 2019 Transonic buffet instability: From two-dimensional airfoils to three-dimensional swept wings. *Physical Review Fluids* .

Richez, F., Lequille, M. & Marquet, O. 2016 Selective frequency damping method for steady rans solutions of turbulent separated flows around an airfoil at stall. *Computers and Fluids* **132**, 51–61.

Sansica, A., Hashimoto, A., Koike, S. & Kouchi, T. 2022 Sidewall effects on the global stability of swept and unswept supercritical wings at buffet conditions. , vol. AIAA Paper 2022-1972.

Sansica, A., Robinet, J.-C., Alizard, F. & Goncalvez, E. 2018 Three-dimensional instability of a flow past a sphere: Mach evolution of the regular and hopf bifurcations. *Journal of Fluid Mechanics* **855**, 1088–1115.

Sharov, D. & Nakahashi, K. 1998 Reordering of hybrid unstructured grids for lower-upper symmetric Gauss-Seidel computations. *AIAA Journal* **36**, 484–486.

Spalart, P. R 2000 Strategies for turbulence modelling and simulation. *International Journal of Heat and Fluid Flow* **21**, 252–263.

Spalart, P. R. & Allmaras, S. R. 1992 A one-equation turbulence model for aerodynamic flows. In *30th Aerospace Sciences Meeting and Exhibit, Aerospace Sciences Meetings*, , vol. AIAA Paper.

Sugioka, Y., Nakakita, K., Koike, S., Nakajima, T., Nonomura, T. & Asai, K. 2021 Characteristic unsteady pressure field on a civil aircraft wing related to the onset of transonic buffet. *Experiments in Fluids* (62:20).

Tezuka, A. & Suzuki, K. 2006 Three-dimensional global linear stability analysis of flow around a spheroid. *AIAA Journal* **44**.

Timme, S 2020 Global instability of wing shock-buffet onset. *Journal of Fluid Mechanics* **885**.

Visbal, M. R. & Gordnier, R. 2000 A high-order flow solver for deforming and moving meshes. , vol. AIAA Paper 2000-2619.